The influence of mobile copper ions on the glass-like thermal conductivity of copper-rich tetrahedrites

Article

Accepted Version

Article

The influence of mobile copper ions on the glass-like thermal conductivity of copper-rich tetrahedrites

Paz Vaqueiro, Gabin Guelou, Andreas Kaltzoglou, Ronald I Smith, Tristan Barbier, Emmanuel Guilmeau, and Anthony V. Powell

Chem. Mater., **Just Accepted Manuscript** • DOI: 10.1021/acs.chemmater.7b00891 • Publication Date (Web): 02 Apr 2017

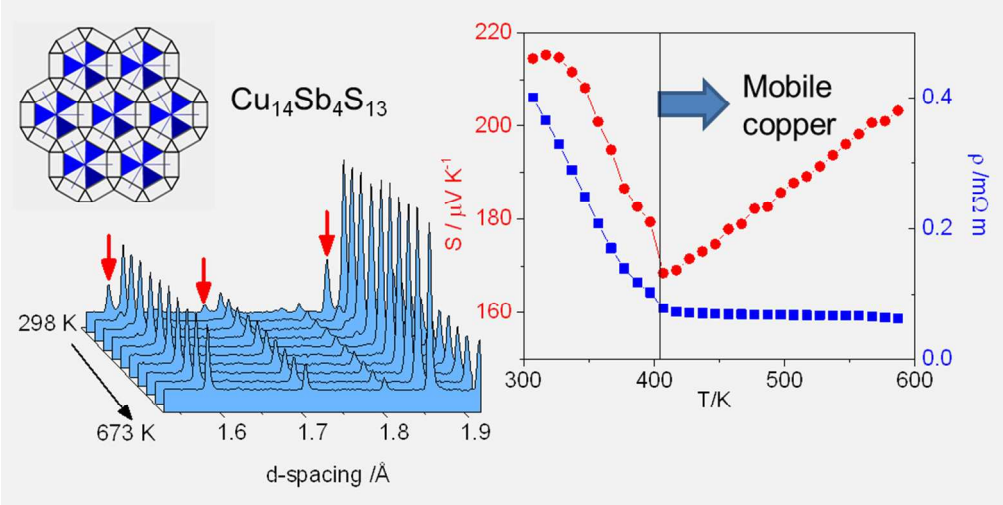

TOC graphic

177x89mm (150 x 150 DPI)

The influence of mobile copper ions on the glass-like thermal conductivity of copper-rich tetrahedrites

Paz Vaqueiro,[a*] Gabin Guélou,[a] Andreas Kaltzoglou,[a] Ronald I. Smith,[b] Tristan Barbier,[c] Emmanuel Guilmeau [c] and Anthony V. Powell[a]

a. Department of Chemistry, University of Reading, Whiteknights, Reading, RG6 6AD, UK.

b. ISIS Facility, Rutherford Appleton Laboratory, Harwell, Oxford, Didcot, OX11 0OX, UK

c. Laboratoire CRISMAT, UMR 6508 CNRS ENSICAEN, 6 bd Maréchal Juin, 14050 CAEN cedex 4, France

ABSTRACT: Tetrahedrites are promising *p*-type thermoelectric materials for energy recovery. We present here the first investigation of the structure and thermoelectric properties of copper-rich tetrahedrites, $Cu_{12+x}Sb_4S_{13}$ ($0 < x \leq 2.0$). At room temperature, all samples with $x > 0$ consist of two tetrahedrite phases. *In-situ* neutron diffraction data demonstrate that on heating, the two tetrahedrite phases coalesce into a single tetrahedrite phase at temperatures between 493 and 553 K, and that this transition shows marked hysteresis on cooling. Our structural data indicate that copper ions become mobile above 393 K. Marked changes in the temperature dependence of the electrical and thermal transport properties of the copper-rich phases occur at the onset of copper mobility. Excess copper leads to a significant reduction in the total thermal conductivity, which for the nominal composition $Cu_{14}Sb_4S_{13}$ reaches a value as low as 0.44 W $m^{-1}K^{-1}$ at room temperature, and to thermoelectric properties consistent with phonon liquid electron crystal (PLEC) behaviour.

1. INTRODUCTION

Thermoelectric devices offer considerable attractions for the recovery of waste heat to produce useful electrical power. For this reason, research efforts worldwide are focused on the search for new thermoelectric materials that overcome the limitations of current materials.[1,2,3] The thermoelectric performance of a material is expressed in terms of a figure of merit, ZT, related to the Seebeck coefficient (S), electrical conductivity (σ) and thermal conductivity (κ) of the material by $ZT = S^2\sigma T/\kappa$. For large scale implementation of thermoelectric energy recovery, the discovery of materials containing abundant, non-toxic and inexpensive elements is essential.

The outstanding thermoelectric performance of materials with the tetrahedrite structure, which are composed predominantly of environmentally-friendly and abundant copper and sulfur, is currently attracting considerable interest.[4] Materials adopting the tetrahedrite structure may be formulated as $A_{10}B_2C_4Q_{13}$ (A = Cu, Ag; B = Mn, Fe, Co, Ni, Zn, Cu, Hg, Cd; C = As, Sb, Bi; Q = S, Se).[5] The crystal structure of the mineral tetrahedrite has been described as a complex defect derivative of the sphalerite structure, in which the transition-metal cations occupy tetrahedral and trigonal-planar sites and the pnictogen atoms occupy trigonal-pyramidal sites.[5] However, the structure of tetrahedrite may also be described as a collapsed sodalite-type tetrahedral framework, formed by transition-metal tetrahedra (Figure 1), where each six-membered window of the sodalite cage contains a CQ_3 trigonal pyramid, and the sodalite cages are filled by sulfide anions octahedrally coordinated to six trigonal planar copper ions, forming a "spinner".[6] This structural description reveals some similarities with those of cage-based thermoelectric materials, such as skutterudites and clathrates.

Naturally-occurring tetrahedrite minerals can be used as a direct source of thermoelectric materials, with figures of merit close to unity at 720 K.[7] The thermoelectric properties of synthetic $Cu_{12-x}TM_xSb_4S_{13}$ (TM= Mn, Fe, Co, Ni, and Zn) have been investigated by a number of groups,[8,9,10,11,12,13] and for instance, ZT~1 is found for $Cu_{11}ZnSb_4S_{13}$ at 720 K.[8] Partial substitution at the pnictogen site with tellurium is also possible, and results in a figure of merit of 0.92 at 723 K for $Cu_{12}Sb_3TeS_{13}$.[14] Selenium can partially replace sulfur up to a composition of $Cu_{12}Sb_4S_{12}Se_2$,[15] and this leads to an enhancement in ZT of almost 40% when compared to $Cu_{12}Sb_4S_{13}$, due to a marked increase in power factor. In addition to the thermoelectric properties at high temperatures, the behaviour of $Cu_{12}Sb_4S_{13}$ at low temperatures is also attracting much interest. On cooling below 85 K, $Cu_{12}Sb_4S_{13}$ undergoes a metal to semiconductor transition, which is accompanied by a structural transition and a drop in the magnetic susceptibility.[16,17]

Studies of the Cu-Sb-S phase diagram indicate that the tetrahedrite structure is found over a wide range of compositions, ranging from ~$Cu_{12}Sb_4S_{13}$ to ~$Cu_{14}Sb_4S_{13}$, with the composition limits being dependent on temperature.[18,19] Although at room temperature samples

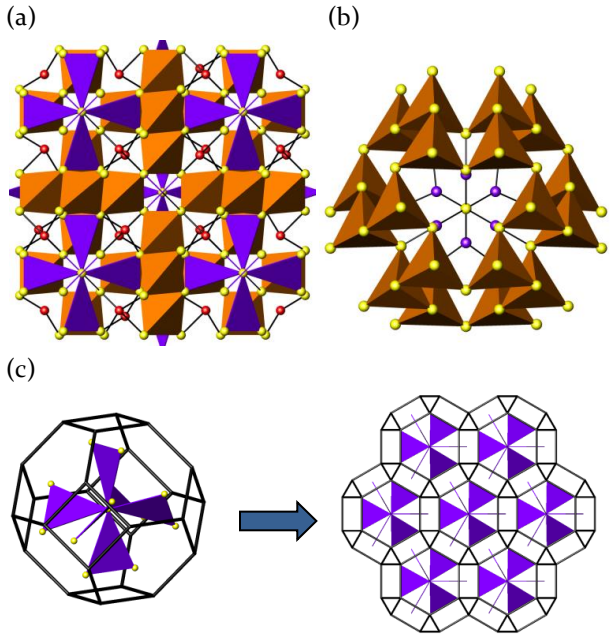

Figure 1. (a) View of the crystal structure of $Cu_{12}Sb_4S_{13}$ along [100], showing the CuS_4 tetrahedra (orange) and the CuS_3 trigonal planar polyhedra (purple). Antimony atoms are shown as red circles, and sulfur atoms as yellow circles. (b) A collapsed sodalite cage in the tetrahedrite structure, viewed along [111], and containing an octahedrally coordinated sulfur at the centre of the cage. The pnictogen atoms have been omitted for clarity. (c) Schematic representation of a sodalite cage, containing the "spinner" formed by the trigonal planar Cu(2) atoms, and of the collapsed sodalite framework viewed along [111]. Each node represents a CuS_4 tetrahedron. For clarity, the SbS_3 units have been omitted.

containing excess copper consist of two tetrahedrite phases, a single-phase region is known to exist at higher temperatures.[18,19] While $Cu_{12}Sb_4S_{13}$ is described as a *p*-type metal with two holes per formula unit, $Cu_{14}Sb_4S_{13}$, with two additional copper atoms per formula unit, is predicted to have a filled valence band and hence exhibit semiconducting behaviour.[20] This feature could be exploited to control the concentration of holes in the valence band of $Cu_{12+x}Sb_4S_{13}$, in a similar way to that achieved by replacing copper with a divalent transition metal (TM) in $Cu_{12-x}TM_xSb_4S_{13}$. However, to the best of our knowledge, the thermoelectric behaviour of tetrahedrites containing excess copper, $Cu_{12+x}Sb_4S_{13}$ ($0 < x \leq 2.0$), has not been investigated. Here, we present the first such investigation of transport property measurements of copper-rich phases, which exhibit phase separation at room temperature. A variable temperature neutron diffraction study of the phase coalescence in copper-rich phases reveals that above 393 K the copper sub-lattice enters a liquid-like state, suggesting that the materials exhibit phonon liquid electron crystal (PLEC) behaviour.

2. EXPERIMENTAL METHODS

2.1 **Synthetic procedures.** Samples with the nominal composition of $Cu_{12+x}Sb_4S_{13}$, where x= 0.3, 1, 1.5 and 2, together with a stoichiometric reference sample ($Cu_{12}Sb_4S_{13}$) were prepared from appropriate mixtures of the elements Cu (Aldrich, 99.5%), Sb (Alfa-Aesar, 99.5%) and S (Aldrich, 99.99+%). Sulfur flakes were dried under vacuum prior to use. The reagents were loaded into fused silica tubes, which were evacuated to $< 10^{-4}$ Torr prior to sealing. The mixtures were heated at 773 K for 2 days before cooling to room temperature at a rate of 1 K min^{-1}. The polycrystalline products were finely ground in air before annealing in evacuated silica tubes at 723 K for 2-4 days. Nominal compositions for all samples are given within quotes.

2.2 **Structural characterisation**. The air-stable polycrystalline products were structurally characterised using a Bruker D8 Advance powder diffractometer, operating with Ge-monochromated Cu Kα1 radiation (λ = 1.5406 Å) and a LynxEye linear detector. Data were collected over the angular range $10 \leq 2\theta/° \leq 120$.

Time-of-flight powder neutron diffraction data were collected from $Cu_{12.3}Sb_4S_{13}$ and $Cu_{14}Sb_4S_{13}$ using the Polaris diffractometer at the ISIS Facility, Rutherford Appleton Laboratory, UK. Powdered samples of each material were sealed into evacuated low-boron content silica ampoules. The ampoules were contained in thin-walled vanadium cans held in a furnace evacuated to a pressure $<10^{-4}$ Torr. Data were collected over the temperature range $300 \leq T/K \leq 673$ K, on heating and on cooling. At selected temperatures, long datasets (300 μAh, approximately 2 hours) were collected, while shorter collection times were used for the remaining runs (80 μAh, approximately 30 min.). Data were also collected on an empty silica ampoule, to enable the subtraction of the amorphous background arising from the glass. 80 μAh datasets were used to determine the temperature evolution of the lattice parameters and the weight fractions of each phase, while 300 μAh datasets were used for full structural determinations. Initial data manipulation and reduction was carried out using the Mantid[21] software package. Neutron diffraction data from the backscattering (average 2θ = 146°) and the ~90° detector banks were summed, normalised and used simultaneously in Rietveld refinement, carried out using the GSAS package.[22]

2.3 **Thermal stability.** The thermal stability of samples with x = 0.3 and 2.0 was investigated using a TA instrument SDT Q600 analyst, which provides simultaneous thermogravimetric and differential heat flow data. Measurements were carried out under a nitrogen flow of 100 mL min^{-1} using heating/cooling steps of ±5 K min^{-1}.

2.4 **Consolidation.** The synthesised powders were consolidated into 12.7 mm diameter pellets using a custom-built hot press, at 723 K for 30 min. A pressure of 80 MPa was applied using a graphite mould with tungsten carbide dies and consolidation was carried out under a constant nitrogen flow to prevent oxidation. Pressure was maintained on cooling until the temperature decreased below 373 K. The densities of the consolidated pellets were measured using an Archimedes balance ADAM PW184 with values ranging from 4.92 g cm^{-3} and 4.99 g cm^{-3}, which correspond to 96 - 99 % of the crystallographic

values. The resulting pellets were polished using a MTI EQ-Unipol-300 grinder/polisher to a thickness of *ca*. 2 mm for physical property measurements.

2.5 **Thermoelectric properties.** The temperature dependence of the electrical resistivity (ρ) and Seebeck coefficient (S) was measured simultaneously over the temperature range 310 ≤ T/K ≤ 580 on a Linseis LSR-3 instrument, under a partial pressure of He. The electrical resistivity was measured with the four-probe DC method using a current of 50 mA between the terminal Pt electrodes and with the axial thermocouple probes separated by a distance of 8.0 mm. For Seebeck coefficient measurements, a constant 50 K temperature gradient was applied.

Thermal transport properties were measured on a Netzsch LFA 447 NanoFlash instrument using Cowan's model[23] with a pulse correction to calculate the thermal diffusivity. The thermal conductivity was calculated using the Dulong-Petit heat capacity.

3. RESULTS AND DISCUSSION

3.1 **Structural characterisation**. Analysis of powder X-ray diffraction data collected at room temperature (Fig. 2) indicates that all samples with x > 0 consist of a mixture of two cubic tetrahedrite phases, with lattice parameters of ~10.32 and ~10.44 Å respectively (see SI). At some compositions, trace amounts of Cu_3SbS_4 (x = 0, 1) or Cu_2S (x =2) are also evident. A range of temperatures and cooling rates (including quenching) were explored, but all synthesis conditions resulted in samples consisting of two tetrahedrite phases. Two distinct tetrahedrite phases persist after hot pressing (SI, Figure S1).

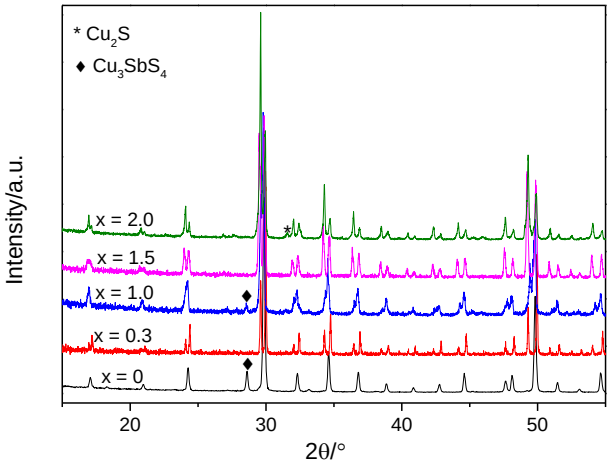

Figure 2. Powder X-ray diffraction patterns collected at room temperature for $Cu_{12+x}Sb_4S_{13}$, showing the presence of two tetrahedrite phases for x > 0. Peaks corresponding to impurities (Cu_3SbS_4 or Cu_2S) are marked.

Powder neutron diffraction data collected on samples with x = 0.3 and x = 2.0 near room temperature are consistent with the results of the analysis of X-ray data, and indicate the presence of two tetrahedrite phases (Figure 3). Comparison with previously reported lattice parameters for tetrahedrites suggests that a ~ 10.32 Å corresponds to a composition of $Cu_{12}Sb_4S_{13}$,[24] while a ~ 10.44 Å is in good agreement with the lattice parameter of a single crystal with composition $Cu_{13.8}Sb_4S_{13}$.[25]

Table 1. Refined parameters for samples with nominal compositions "$Cu_{12.3}Sb_4S_{13}$" and "$Cu_{14}Sb_4S_{13}$", determined using neutron diffraction data collected at 323 and 298 K respectively. Phase 1 is a stoichiometric tetrahedrite, $Cu_{12}Sb_4S_{13}$, and phase 2 is a copper-rich tetrahedrite, $Cu_{12+x}Sb_4S_{13}$. Space group $I\bar{4}3m$ and atomic positions: Cu(1) on 12*d* (1/4,1/2,0); Cu(2) on 12*e* (*x*,0,0) for the majority phase and on 24*g* (*x*,*y*,-*y*) for the minority phase; Cu(3) on 24*g* (*x*,*x*,*z*); Sb(1) on 8*c* (*x*,*x*,*x*); S(1) on 24*g* (*x*,*x*,*z*); S(2) on 2*a* (0,0,0). SOF: site occupancy factor.

		"$Cu_{12.3}Sb_4S_{13}$"		"$Cu_{14}Sb_4S_{13}$"	
Phase		1	2	1	2
a / Å		10.32161(3)	10.4449(1)	10.3194(1)	10.43675(5)
Cu(1)	U_{iso}/Å²	0.0192(3)	0.029(1)	0.019(1)	0.029(1)
	SOF	1.0	1.0	1.0	0.926(16)
Cu(2)	x	0.2184(2)	0.2166(7)	0.2180(6)	0.2146(3)
	y	0.0(-)	0.0223(6)	0.0199(5)	0.0
	U_{iso}*/Å²	0.059	0.029(1)	0.019(1)	0.062
	SOF	0.975(9)	0.5(-)	0.5(-)	0.947(13)
Cu(3)	x	-	0.284(2)	-	0.2870(9)
	z	-	0.024(4)	-	0.029(2)
	U_{iso}/Å²	-	0.029(1)	-	0.089(10)
	SOF	-	0.10	-	0.146(6)
Sb(1)	x	0.2690(1)	0.2683(8)	0.2696(6)	0.2667(4)
	U_{iso}/Å²	0.0138(5)	0.021(3)	0.011(2)	0.024(1)
S(1)	x	0.1153(2)	0.113(1)	0.1168(9)	0.1147(4)
	z	0.3634(3)	0.363(1)	0.363(1)	0.3616(5)
	U_{iso}/Å²	0.0133(4)	0.016(2)	0.009(1)	0.018(1)
S(2)	U_{iso}/Å²	0.016(1)	0.016(2)	0.009(1)	0.009(2)
Weight fract./%		77.4(1)	22.6(2)	21.4(1)	73.4(3)
Cu_2S/wt%		-		5.2(1)	
χ^2		1.06		1.43	
90° bank R_{wp} /%		1.05		1.17	
backscattering bank R_{wp} / %		1.19		1.36	

*Anisotropic U_{ij} values were converted to a single equivalent U_{iso}, which is tabulated here.

Rietveld refinements using the reported structural models for $Cu_{12}Sb_4S_{13}$ and $Cu_{13.8}Sb_4S_{13}$,[24,25] which differ in the presence of an additional copper site in the copper rich phase, result in a good agreement between observed and calculated profiles, reflected in low residuals (Table 1). Constraints were introduced for the thermal parameters of the minority tetrahedrite phase: a single thermal

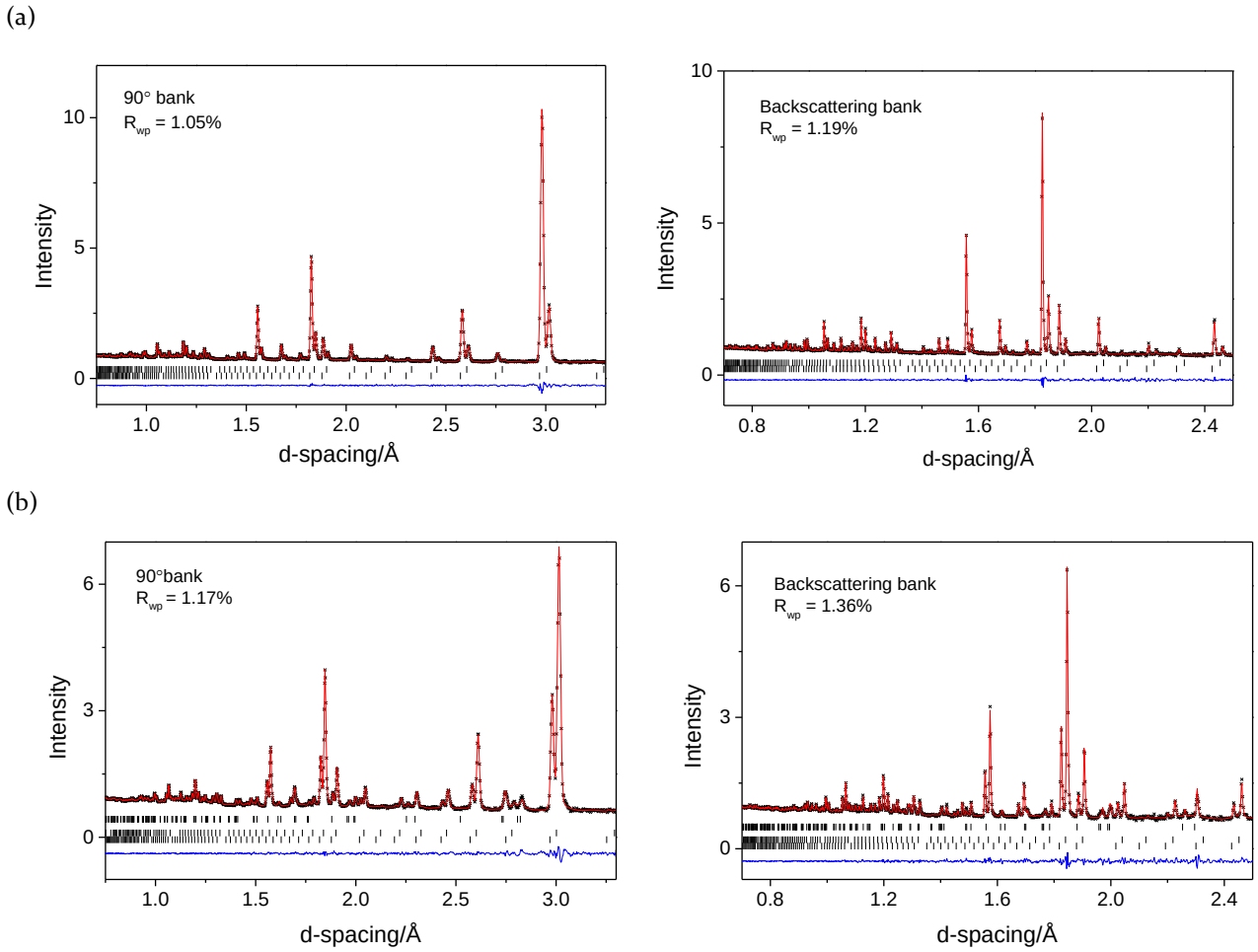

Figure 3. Final observed (crosses), calculated (red solid line) and difference (lower full line) profiles from Rietveld refinement using neutron powder diffraction data from the ~90° and backscattering detector banks for samples of nominal composition (a) "$Cu_{12.3}Sb_4S_{13}$" at 323 K, and (b) "$Cu_{14}Sb_4S_{13}$" at 298 K. In (a) top and bottom markers correspond to $Cu_{12+x}Sb_4S_{13}$ and $Cu_{12}Sb_4S_{13}$, respectively. In (b), top, middle and bottom markers correspond to $Cu_{2-x}S$, $Cu_{12+x}Sb_4S_{13}$ and $Cu_{12}Sb_4S_{13}$, respectively.

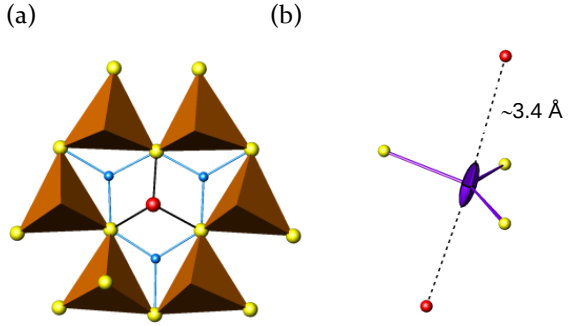

Figure 4. (a) A window of the sodalite cage in the tetrahedrite structure, showing the location of the Cu(3) atoms; (b) the anisotropic thermal ellipsoid of the Cu(2) site. $Cu(1)S_4$ tetrahedra are shown in orange, Cu(2) as purple ellipsoids, Cu(3) atoms as light blue circles, antimony as red circles and sulfur as yellow circles.

parameter was used for the copper sites, and a single thermal parameter was used for the two sulfur sites. Initial refinements for site occupancy factors (SOFs) of the copper atoms in the majority phase resulted in values close to unity and therefore these were subsequently fixed at this value. For the majority tetrahedrite phase, isotropic atomic displacement parameters (ADP) were used, with the exception of that for the trigonal planar Cu(2) site, which was modelled anisotropically. For the minority tetrahedrite phase, the approach described by Andreasen et *al.*[26] to model the trigonal planar Cu(2) site was used, in order to reduce the number of independent parameters. In this case, the trigonal planar Cu(2) atom, which was originally on a 12*e* site, with coordinates (*x*, 0, 0), was split into two (*x*, *y*, -*y*) positions above and below the plane formed by the three sulfur atoms. This split 24*g* site was assigned a site occupancy factor of 0.5, while the Cu(3) site occupancy was fixed at 0.1, based on the previously reported model for the copper-rich tetrahedrite $Cu_{13.8}Sb_4S_{13}$.[25]

Rietveld refinements indicate the sample of nominal composition "$Cu_{12.3}Sb_4S_{13}$" consists of a mixture of two tetrahedrites with the crystallographically-determined compositions $Cu_{11.85(5)}Sb_4S_{13}$ and $Cu_{12.6}Sb_4S_{13}$, with weight percentages of 77% and 23% respectively. Similarly "$Cu_{14}Sb_4S_{13}$" is a mixture of 21 wt% of $Cu_{12}Sb_4S_{13}$ and 73 wt% of $Cu_{13.0(1)}Sb_4S_{13}$, together with *ca.* 5 wt% of Cu_2S.

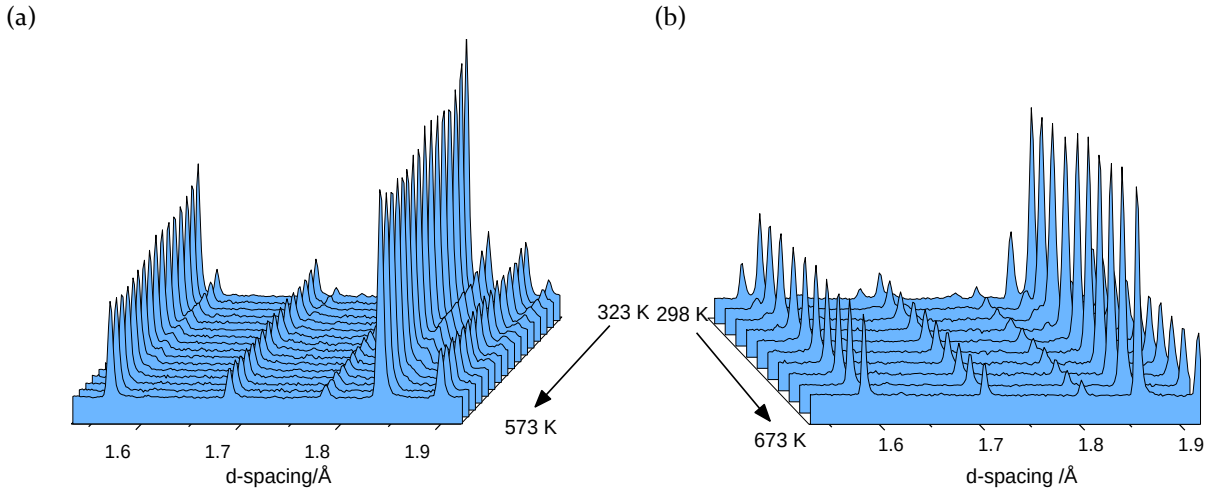

Figure 5. Neutron diffraction patterns collected in the backscattering bank over the d-spacing range $1.5 \leq d/Å \leq 1.94$ for samples of nominal composition (a) "$Cu_{12.3}Sb_4S_{13}$" and (b) "$Cu_{14}Sb_4S_{13}$" on heating.

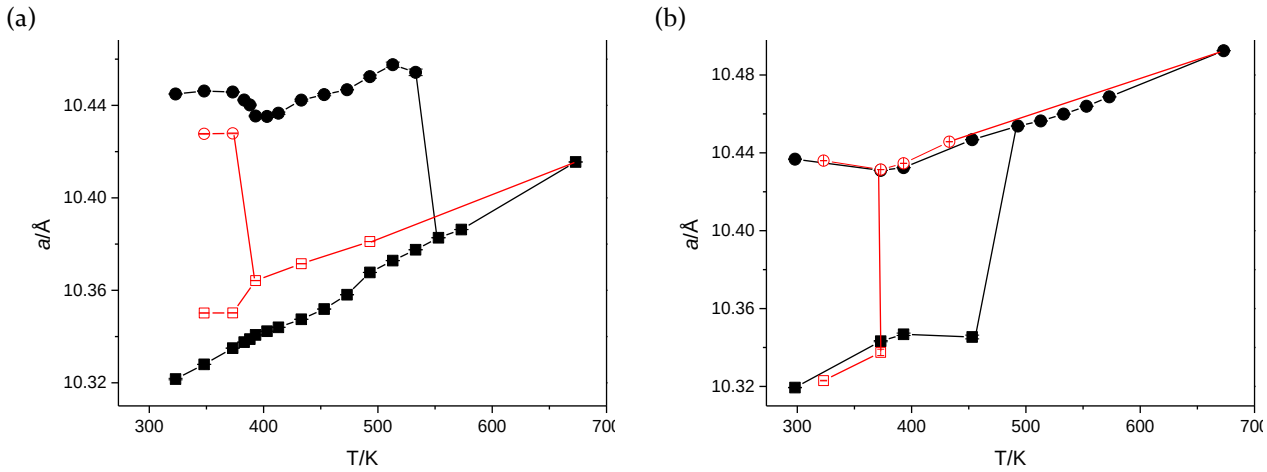

Figure 6. Temperature dependence of the lattice parameters for samples of nominal composition (a) "$Cu_{12.3}Sb_4S_{13}$" and (b) "$Cu_{14}Sb_4S_{13}$". Phase 1 is shown as squares, and phase 2 as circles. Black solid symbols indicate values determined on heating, while red open symbols correspond to those determined on cooling.

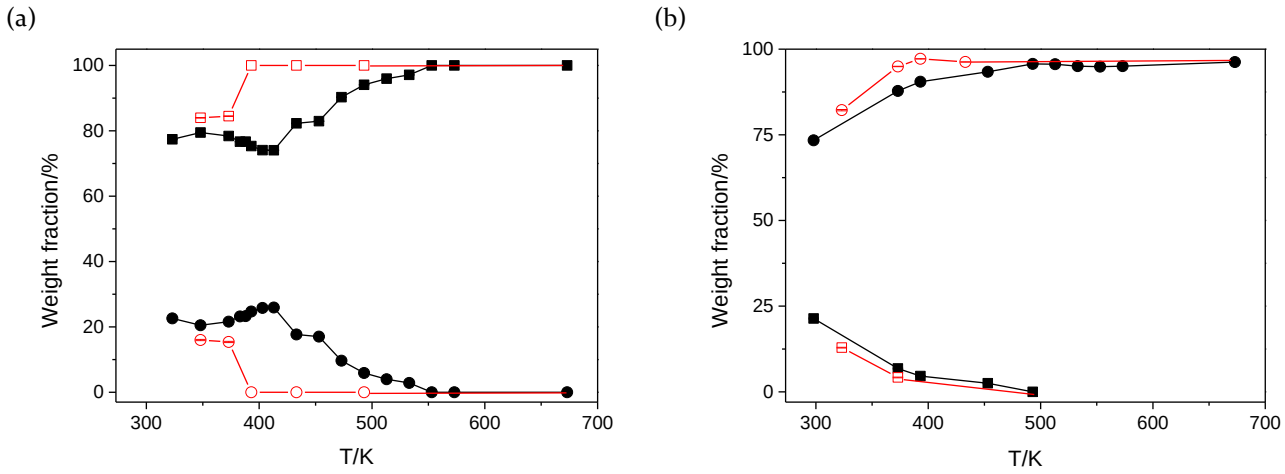

Figure 7. Temperature dependence of the weight fractions of the two tetrahedite phases for samples of nominal composition (a) "$Cu_{12.3}Sb_4S_{13}$" and (b) "$Cu_{14}Sb_4S_{13}$". Phase 1 is shown as squares, and phase 2 as circles. Black solid symbols indicate values determined on heating, while red open symbols correspond to values determined on cooling.

In both cases, there is good agreement between the nominal copper content of the sample and the overall amount of copper calculated from the determined compositions arising from the Rietveld refinements. The most significant difference between the two tetrahedrite phases lies in the existence of a partially occupied Cu(3) site in the copper-rich phase, in which copper is in trigonal-planar coordination, with three sulfur atoms at distances of 2.154(12)-2.27(2) Å. These relatively short Cu-S distances are comparable with those found for other sulfides containing three-coordinate copper, such as CuS (2.19 Å).[27] This Cu(3) site is located in the windows of the sodalite cages (Figure 4(a)), with an overall occupancy of 15% at room temperature. Occupation of the Cu(3) site in the tetrahedrite phase with the smaller lattice parameter would result in anomalously short Cu-S bond lengths at this site. Selected bond distances for both tetrahedrite phases have been included in the SI. The Cu(1)-S distances are similar to those found for other materials containing CuS_4 tetrahedra,[28] while the bond distances in the SbS_3 trigonal pyramids are similar to those in skinnerite, Cu_3SbS_3.[29] Comparison of bond distances for the two tetrahedrite phases reveals an elongation, by approximately 1.7%, of the Cu(1)-S bonds, while the Sb-S bonds, in comparison, increase only by 0.3% from $Cu_{12}Sb_4S_{13}$ to $Cu_{12+x}Sb_4S_{13}$. In both phases, the long axis of the thermal ellipsoid for Cu(2) is perpendicular to the plane formed by three sulfur atoms, and points towards two antimony atoms located in opposite windows of the sodalite cage (Figure 4(b)).

Neutron diffraction data collected as a function of temperature up to 673 K, with the samples encapsulated in silica ampoules to avoid changes in composition, reveal major structural changes (Figures 5, 6 and 7). On heating "$Cu_{12.3}Sb_4S_{13}$" two tetrahedrite-type phases are observed up to 553 K, while above this temperature, a single tetrahedrite phase is found (Figure 5(a)). This phase transition exhibits a significant degree of hysteresis: it is necessary to cool to 373 K to detect the reappearance of two tetrahedrite phases (Figure 6(a)). For "$Cu_{14}Sb_4S_{13}$" data were collected in coarser steps (Figure 5(b)), but the behaviour is similar, with the coalescence of the two tetrahedrite phases into one occurring at 493 K on heating, and the reappearance of two phases at 373 K on cooling (Figure 6(b)). In addition, during the process of heating "$Cu_{14}Sb_4S_{13}$", the trace phase of tetragonal Cu_2S[30] transforms into cubic digenite[31] at 453 K. The later phase remains present in the sample up to the highest temperature investigated (673 K). In both samples, the temperature dependence of the lattice parameters (Figure 6) of both tetrahedrites shows an anomaly around 393 K, which is accompanied by a change in the linear thermal expansion coefficient. For instance, for "$Cu_{14}Sb_4S_{13}$", the linear expansion coefficients below 373 K are -7.38×10^{-6} K^{-1} and 3.08×10^{-5} K^{-1} for the majority and minority phases respectively, whilst above 393 K a value of 1.99×10^{-5} K^{-1} is found for the majority phase. In both samples, at temperatures above 400 K, peaks from both tetrahedrite phases show significant overlap and broadening. For samples with a large copper excess, DSC data (Figure 8) exhibit a weak endothermic peak at *ca*. 393 K, the temperature at which the anomaly in lattice parameters is observed. This DSC transition was previously reported by Tatsuka and Morimoto, who attributed it to the presence of skinnerite.[18] This is however not consistent with our powder neutron diffraction data, where no evidence for skinnerite is found.

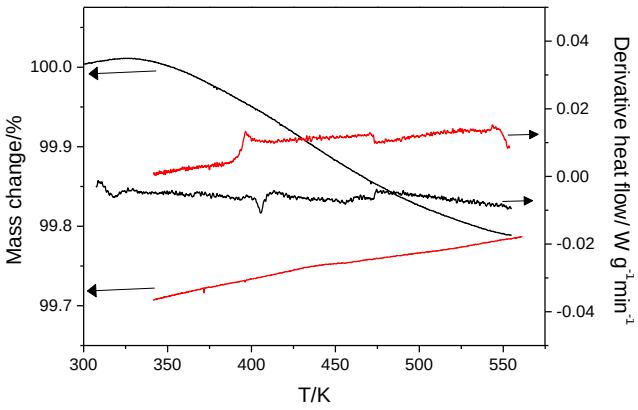

Figure 8. Thermogravimetric and DSC curves for $Cu_{14}Sb_4S_{13}$ on heating (black line) and on cooling (red line).

In a previous study of the Cu-Sb-S phase diagram, the temperature at which the two tetrahedrite phases coalesce into a single tetrahedrite, which can be described as the exsolution temperature, was determined to be around 393 K, using data collected with a Weissenberg camera.[32] Tatsuka and Morimoto reported that exsolution of the two tetrahedrite phases into a single tetrahedrite occurs at temperatures as low as 368 K.[18] However, our *in-situ* study unequivocally demonstrates that the two tetrahedrite phases persist up to much higher temperatures (553-493 K, depending on composition), and that the transition shows marked hysteresis on heating and cooling. Possible sulfur loss, due to incomplete sealing of the samples in previous studies, together with the marked overlap and broadening of peaks that is evident in our measurements above 400 K may have made detection of the two tetrahedrite phases difficult in earlier studies. Recently, it has been shown that substitution of Sb by Te in $Cu_{12}Sb_{4-x}Te_xS_{13}$ ($1 \leq x \leq 1.75$) lowers the exsolution temperature to 250 K.[33]

Results of Rietveld refinements using data collected at the highest temperature investigated are presented in Table 2, while those for data collected at intermediate temperatures can be found in the SI. In each case, the structural model for the majority tetrahedrite phase found below the exsolution temperature was used, and the site occupancy factors of the copper atoms were allowed to refine. Rietveld refinements using a single tetrahedrite phase (Figure 9) result in excellent agreement between experimental and calculated data. These Rietveld

refinements indicate that at 673 K the sample with nominal composition "$Cu_{12.3}Sb_4S_{13}$" consists of a single tetrahedrite phase, with a crystallographically determined composition of $Cu_{11.6(1)}Sb_4S_{13}$, while the "$Cu_{14}Sb_4S_{13}$" sample contains primarily a tetrahedrite with the composition $Cu_{11.7(2)}Sb_4S_{13}$, together with *ca*. 4wt% of Cu_2S (digenite). Diffraction data (Figure 9) indicate that no other copper-containing phase, such as copper metal, is present, and in the single-phase region, the lattice parameters increase with increasing temperature (Figure 6). Although the samples are contained in sealed silica tubes, the crystallographically-determined copper content is much lower than that expected on the basis of the nominal composition. In particular, approximately 0.7 and 2.3 copper atoms per formula unit appear to be "missing" for the samples with nominal compositions "$Cu_{12.3}Sb_4S_{13}$" and "$Cu_{14}Sb_4S_{13}$" respectively. The site occupancy factors for the copper atoms decrease with increasing temperature, and a drop is observed for Cu(1) in the copper-rich phase of "$Cu_{14}Sb_4S_{13}$" between 373 and 493 K. Difference Fourier maps (see SI) were calculated to identify potential interstitial sites in which the remaining copper might be located. However, examination of these maps indicates that, although at 673 K there is residual nuclear density, there are no clear local maxima; a finding consistent with the presence of highly disordered atoms in the structure.

Examination of the Fourier maps for data collected at different temperatures indicates that residual nuclear densities are negligible below 393 K, whilst above this temperature significant residual density distributed throughout the unit cell is evident. Furthermore, bond lengths do not increase linearly with temperature (Tables S9 and S10, SI). In particular, the Sb-S distances change very little up to 393 K, followed by a sharp increase between 393 and 493 K, while the Cu(1)-S distances increase more rapidly above 393 K. These discontinuities in bond lengths occur at the same temperature as the anomalies in lattice parameters, the endothermic peak in the DSC measurements and the appearance of residual nuclear density in the Fourier maps. All of these indicate that a structural transition, involving a change from localised to mobile copper ions, occurs at 393 K. Similar transitions have been observed in Cu_3SbS_3, Cu_3BiS_3 and Cu_3SbSe_3, and have also been attributed to the onset of copper mobility, which occurs at relatively low temperatures, ranging between 395 and 423 K.[34,35,36] The decomposition on cooling of the high-temperature tetrahedrite phase into two distinct phases, with identical Sb and S content, would seem to proceed by diffusion of copper atoms. Quenching these materials into the two-phase region may lead to fluctuations of the copper concentration, and this may result in a spinodal decomposition.

There are also striking differences in the magnitude and temperature dependence of the ADPs (Figure 10). In particular, those for Cu(2) and Cu(3) are considerably larger than those for sulfur and antimony, and have a stronger temperature dependence (SI, Tables S4 and S7). Although

Table 2. Refined parameters for samples of nominal composition "$Cu_{12.3}Sb_4S_{13}$" and "$Cu_{14}Sb_4S_{13}$", determined using neutron diffraction data diffraction data collected at 673 K. Space group $I\bar{4}3m$ and atomic positions: Cu(1) on 12*d* (1/4,1/2,0); Cu(2) on 12*e* (*x*,0,0); Cu(3) on 24*g* (*x*,*x*,*z*), Sb(1) on 8*c* (*x*,*x*,*x*), S(1) on 24*g* (*x*,*x*,*z*), S(2) on 2*a* (0,0,0). SOF: site occupancy factor.

		"$Cu_{12.3}Sb_4S_{13}$"	"$Cu_{14}Sb_4S_{13}$"
a / Å		10.41304(4)	10.49246(4)
Cu(1)	U_{iso}/Å^2	0.055(1)	0.064(1)
	SOF	0.973(15)	0.86(2)
Cu(2)	*x*	0.2169(3)	0.2152(3)
	U_{iso}^*/Å^2	0.099	0.106
	SOF	0.96(1)	0.87(1)
Cu(3)	*x*	-	0.280(1)
	z	-	0.041(3)
	U_{iso}/Å^2	-	0.14(3)
	SOF	-	0.108(9)
Sb(1)	*x*	0.2663(2)	0.2659(3)
	U_{iso}/Å^2	0.032(1)	0.039(1)
S(1)	*x*	0.1134(4)	0.1137(5)
	z	0.3631(5)	0.3605(6)
	U_{iso}/Å^2	0.029(1)	0.037(1)
S(2)	U_{iso}/Å^2	0.025(2)	0.021(2)
Weight fract. / %		100	96.24(6)
Cu_2S / wt%		-	3.76(9)
χ^2		1.13	1.01
~90° Bank Rwp / %		1.14	1.13
Backscattering bank Rwp / %		1.15	1.06

*Anisotropic U_{ij} values were converted to a single equivalent U_{iso}, which is tabulated here.

the ADP for Cu(1) near room temperature is only 30% larger than those of sulfur and antimony, its temperature dependence is similar to that of Cu(2). At temperatures above the Debye temperature, the Einstein temperature[37] of the copper atoms can be determined according to:

$$U_{iso} = \frac{h^2 T}{m k_B \theta_E^2 4\pi^2}$$

where h and k_B are the Plank and Boltzmann constants, m is the mass and θ_E is the Einstein temperature of the oscillator. The Einstein temperatures, determined from the slope of a plot of $U_{iso/eq}$ *vs*. temperature, for the majority phase in "$Cu_{12.3}Sb_4S_{13}$" are 87 and 79 K for Cu(1) and Cu(2), while for the majority phase in "$Cu_{14}Sb_4S_{13}$" the Einstein temperatures are 91 and 79 K, respectively. These

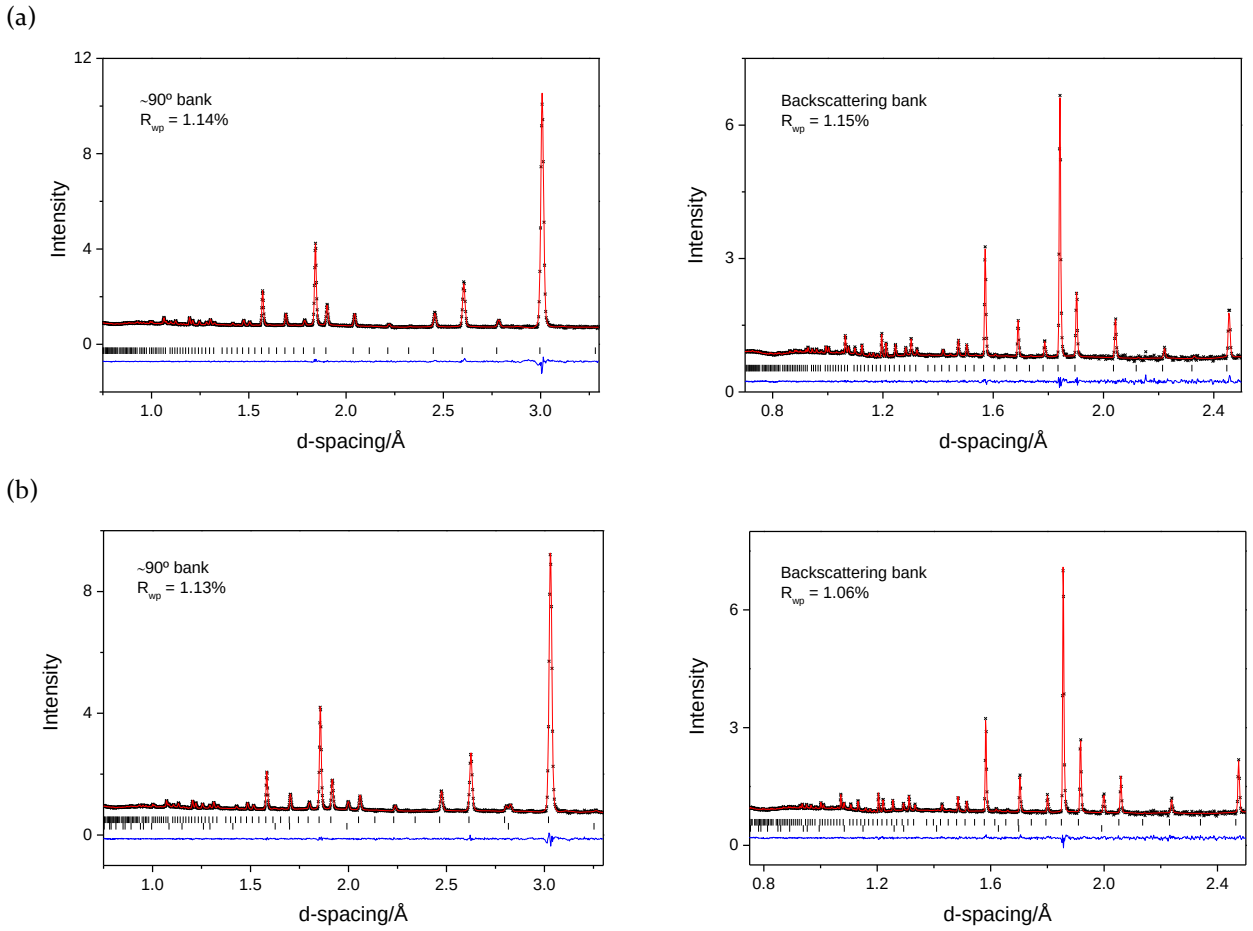

Figure 9. Final observed (crosses), calculated (red solid line) and difference (lower full line) profiles from Rietveld refinement using neutron powder diffraction data from the ~90° and backscattering detector banks for samples of nominal composition (a) "$Cu_{12.3}Sb_4S_{13}$" and (b) "$Cu_{14}Sb_4S_{13}$" at 673 K. In (a) reflection markers for tetrahedrite are shown, while in (b), top and bottom markers correspond to $Cu_{12+x}Sb_4S_{13}$ and $Cu_{2-x}S$ respectively.

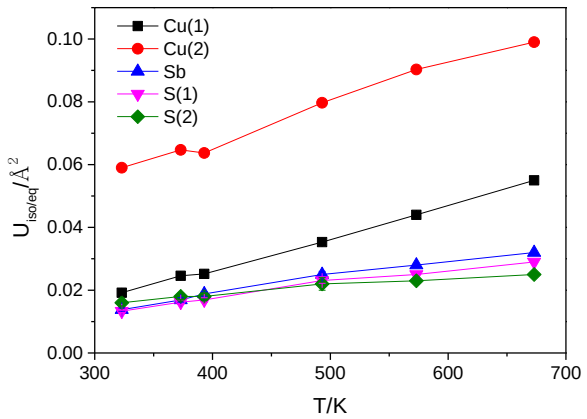

Figure 10. Temperature dependence of the ADPs for the majority phase in "$Cu_{12.3}Sb_4S_{13}$". Error bars are within the points.

values are comparable with those determined for the trigonal planar copper site in stoichiometric tetrahedrites, using powder X-ray diffraction data collected at lower temperatures.[9] This is also broadly consistent with the analysis of low-temperature heat capacity data for stoichiometric tetrahedrites, which have been described with a Debye term and three Einstein oscillators with characteristic temperatures of 12, 33 and 97 K, ascribed to displacements of the trigonal planar copper atoms.[38] In stoichiometric tetrahedrite, the large ADP of the trigonal planar copper has been attributed to a low-energy vibration of this atom out of the CuS_3 triangular plane.[9] It has been proposed that weak out-of-plane bonding, induced by the lone-pair electrons of the antimony atoms, is responsible for this rattling mode.[39] By contrast, in the ionic conductor Cu_3SbSe_3, the large ADPs of the copper atoms are related to their weak bonding within the rigid Sb-S framework.[40] Calculations show that in Cu_3SbSe_3, copper atoms are able to diffuse within a one-dimensional channel, and this results in a low-frequency vibrational mode.[40] In the case of the copper-rich tetrahedrites, the structural data presented here demonstrates that the copper sublattice above 393 K contains mobile copper ions and is in a liquid-like state. Hence the structural behaviour of copper-rich tetrahedrites parallels that of Cu_3SbSe_3. Given the relatively short Cu(3)-Cu(1) and

Cu(3)-Cu(2) distances of 2.37(2) and 3.05(2) Å respectively, it is likely that the diffusion path for the Cu ions in the copper-rich phases involves the interstitial Cu(3) site, which is located in the windows of the sodalite cages. By contrast, a similar neutron diffraction analysis for stoichiometric "$Cu_{12}Sb_4S_{13}$" indicates that copper is not mobile at elevated temperatures.[41,42]

3.2 **Thermoelectric properties**. Thermogravimetric data (Figure 8) collected under a flowing nitrogen atmosphere indicates that relatively little mass loss occurs (< 0.3% for "$Cu_{12.3}Sb_4S_{13}$" and < 0.04% for "$Cu_{14}Sb_4S_{13}$") upon heating the samples up to 573 K, hence transport measurements have been carried out up to this temperature. All samples exhibit *p*-type behaviour, as evidenced by the positive sign of the Seebeck coefficient (Figure 11). The temperature dependence of the electrical resistivity (ρ) and the Seebeck coefficient for all copper-rich samples show two distinct regions of behaviour (Figure 11), with a transition temperature which rises from 375 to 410 K with increasing copper content. This transition, which is absent for the stoichiometric "$Cu_{12}Sb_4S_{13}$" tetrahedrite, occurs at the onset of copper mobility that we have established by powder neutron diffraction. Below this transition, the temperature dependence of the electrical resistivity is characteristic of semiconducting behaviour, whilst above the transition it exhibits a very weak temperature dependence, similar to that of "$Cu_{12}Sb_4S_{13}$". The Seebeck coefficient exhibits a linear temperature dependence above the transition. Marked discontinuities in the electrical transport properties are not apparent at the exsolution temperature, above which a single tetrahedrite phase exists. A change in the temperature dependence of the electrical conductivity and Seebeck coefficient has been previously observed at the temperature at which ions become mobile for ionic conductors such as $CuCrSe_2$,[43] Cu_7PSe_6[44] or Ag_8SnSe_6.[45] Above this transition temperature, there is an ionic contribution to the resistivity and the Seebeck coefficient, as well as the electronic contribution. Although the Seebeck coefficient increases markedly with increasing copper content, the electrical resistivity also increases. Consequently, the power factor of copper-rich tetrahedrites is lower than that of stoichiometric tetrahedrite (Figure 11). With increasing x, the power factor decreases up to x = 1, before increasing again for x = 1.5 and 2, primarily due to the large increase in Seebeck coefficient.

The introduction of additional copper atoms has a marked effect on the thermal diffusivity (SI, Figure S8) and hence the thermal conductivity (Figure 12), with the lowest values obtained for the most copper-rich members of the series. The thermal diffusivity reaches values as low as 0.2 $mm^2 s^{-1}$ at room temperature, comparable to values found for superionic conductors.[45] The total thermal conductivity decreases by 66%, from a value of 1.3 $W m^{-1} K^{-1}$ for stoichiometric tetrahedrite at room-temperature to 0.44 $W m^{-1} K^{-1}$ for "$Cu_{14}Sb_4S_{13}$". The lattice thermal conductivity (SI, Figure S9) at room temperature, estimated using the electrical resistivity data in conjunction with the Wiedemann-Franz law (with a Lorenz constant of 2.45 x 10^{-8} W Ω K^{-2}), also shows a marked reduction with increasing copper content. The low thermal conductivity of stoichiometric tetrahedrites is often attributed to the out-of-plane vibrations of the trigonal planar Cu(2) atoms in the "spinner".[9] However, the existence of two phases below the exsolution temperature may be providing an additional source of phonon scattering, and this would explain the drop in lattice thermal conductivity when compared to the stoichiometric phase.

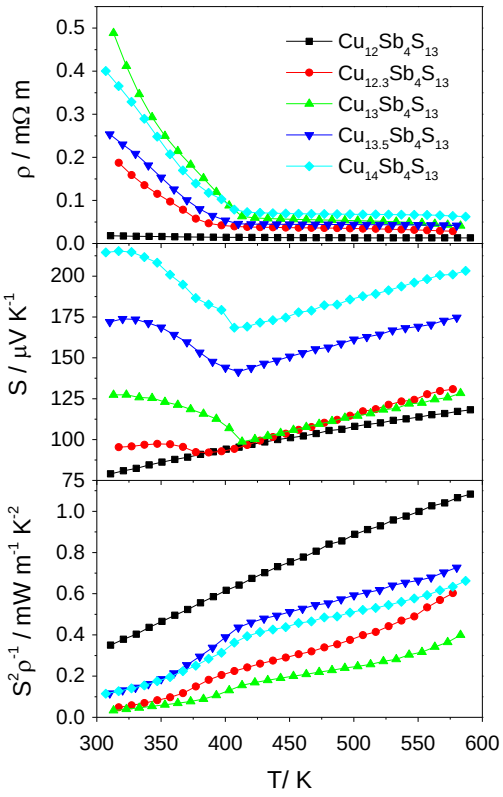

Figure 11 Resistivity, Seebeck coefficient and power factor for "$Cu_{12+x}Sb_4S_{13}$" (0 ≤ x ≤ 2.0) as a function of temperature.

The thermal conductivity and the thermal diffusivity show a clear step at the same temperature (*ca*. 400 K) at which the electrical resistivity shows a transition due to the onset of copper mobility. Below this transition, the electronic contribution to the thermal conductivity is almost negligible (SI, Figure S9) due to the high electrical resistivity, whilst above this temperature κ_{el} is a significant contributor to the total thermal conductivity. The lattice thermal conductivity of the copper-rich tetrahedrites is nearly temperature independent. For samples with x > 1, the lattice thermal conductivity is below the minimum thermal conductivity at the amorphous limit, κ_{min}, which for $Cu_{12}Sb_4S_{13}$ has been estimated as approximately 0.5 $W m^{-1} K^{-1}$ at 300 K,[46] using the approach pro-

posed by Cahill.[47] Very low thermal conductivities, with values below the glassy limit (κ_{min}) have been observed for phonon-liquid electron crystal (PLEC) materials,[44] where the presence of a liquid-like cation sublattice containing highly mobile ions leads to a softening of the phonon modes. This type of behaviour would be consistent with the conclusions arising from our structural study of the copper-rich tetrahedrites, which indicates that the copper ions are highly mobile. Moreover, the low Einstein temperatures found for the copper atoms in these copper-rich phases correspond to low-frequency phonon vibrational modes, ranging between 55 and 63 cm^{-1}. A liquid-like state of the copper ions would result in a very short phonon mean free path, and hence in values of the lattice thermal conductivity near the glass limit.

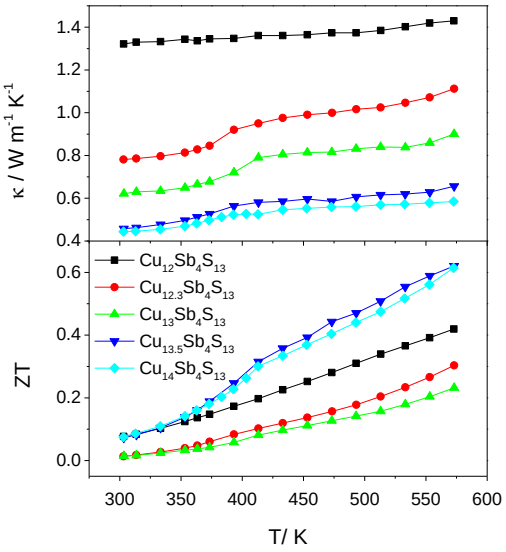

Figure 12 Thermal conductivity and figure of merit for "$Cu_{12+x}Sb_4S_{13}$" ($0 \le x \le 2.0$) as a function of temperature.

For most crystalline materials the lattice thermal conductivity is strongly dependent on temperature, and exhibits a T^{-1} trend at high temperatures.[48] Although the tetrahedrites reported here are crystalline materials, their thermal conductivity is glass-like. In a previous study of stoichiometric tetrahedrites, the temperature dependence at T < 10 K of thermal conductivity and heat capacity has been compared to that of type-I clathrates.[49] For materials consisting of a host lattice containing guest atoms, resonant phonon scattering may occur through the coupling of lattice acoustic modes with localised low-frequency optical modes of the guest atoms.[48] It has been suggested that this mechanism not only reduces the thermal conductivity in cage compounds like skuterudites,[50] but could also play a significant role in materials with dynamic disorder of ions, as this disorder will give rise to low-energy optical phonon modes. This mechanism could explain the glass-like thermal conductivity of stoichiometric tetrahedrites, as well as that of the copper-rich phases, which contain mobile copper ions above 393 K.

The thermoelectric figure of merit, ZT, of copper-rich tetrahedrites reaches optimal values for x = 1.5 and x = 2.0 (Figure 12), due to the low thermal conductivity of these materials. The value of ZT = 0.62 obtained for "$Cu_{14}Sb_4S_{13}$" at 573 K is remarkably similar to those previously reported for a range of substituted tetrahedrites, including $Cu_{10.4}Ni_{1.6}Sb_4S_{13}$,[13] $Cu_{11}ZnSb_4S_{13}$[8] and $Cu_{12}Sb_3TeS_{13}$,[46] all of which reach ZT ~ 0.6 at 573 K, and clearly demonstrates that copper excess is an effective strategy to optimise the thermoelectric performance of tetrahedrites. Given the increasing trend of the power factor and the weak temperature dependence of the thermal conductivity, we expect that ZT for the copper-rich phases will rise with increasing temperature, and extrapolation of our data for "$Cu_{14}Sb_4S_{13}$" leads to ZT ~ 1.0 at 720 K. Concerns about sample stability, owing to possible copper diffusion from the sample into the instrument electrodes, have precluded measurements to higher temperatures.

4. CONCLUSIONS

Our *in-situ* diffraction study provides clear evidence for the coexistence of a nearly stoichiometric and a copper-rich tetrahedrite phase over a wide range of temperatures and compositions, which coalesce to a single tetrahedrite phase at temperatures between 493 and 553 K. Significantly, this study demonstrates that copper becomes mobile above 393 K, and that the materials are likely to be superionic conductors in this temperature range. Measurements of ionic conductivity would be desirable to confirm this. Analysis of the copper ADPs has enabled the identification of low-energy phonon modes, associated with the liquid-like copper sublattice. Strong phonon scattering arising from the presence of a liquid-like copper sublattice results in an exceptionally low thermal conductivity, consistent with phonon liquid electron crystal (PLEC) behaviour. The thermoelectric figure of merit of these materials reaches values comparable with those of stoichiometric tetrahedrites at the same temperature. We have shown, for the first time, that non-stoichiometric tetrahedrites offer exciting opportunities in the search for thermoelectric materials. Given that the tetrahedrite structure is found over a wide range of compositions, $Cu_{12+x}Sb_{14+y}Sb_{13}$,[18,19] further studies of non-stoichiometric phases will be needed. The effect of substitution at the cation or anion sites in $Cu_{12+x}Sb_4S_{13}$ should also be investigated, as substitution could lower the exsolution temperature and provide a mechanism to control copper mobility.

ASSOCIATED CONTENT

Supporting Information. Le Bail refinements for powder X-ray data, Rietveld refinements for neutron diffraction data, difference Fourier maps, lattice parameters, bond distances, thermal diffusivity and lattice and electronic thermal con-

ductivities. This material is available free of charge via the Internet at http://pubs.acs.org.

AUTHOR INFORMATION

Corresponding Author

* E-mail: p.vaqueiro@reading.ac.uk

Funding Sources

Financial support from the European Commission (FP7-SME-2012-1, Grant Agreement No. 315019) is gratefully acknowledged. Neutron scattering beamtime at ISIS was provided by the UK Science and Technology Facilities Council (STFC).

ACKNOWLEDGMENT

The authors wish to thank the University of Reading for financial support for GG and for access to the Chemical Analysis Facility for powder X-ray diffraction and TGA/DSC.

Table of Contents Graphic

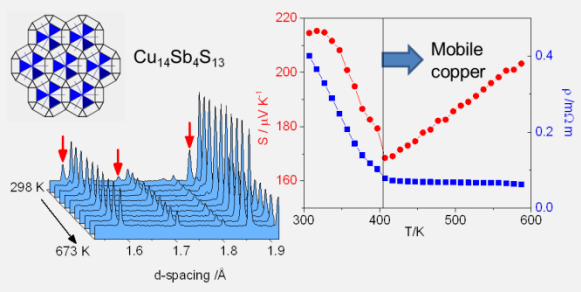

REFERENCES

1 Sootsman, J.; Chung, D.; Kanatzidis, M. G. New and Old Concepts in Thermoelectric Materials *Angew. Chem. Int. Ed.* **2009**, *48*, 8616–8639.

2 Gonçalves, A.P.; Godart, C. New Promising Bulk Thermoelectrics: Intermetallics, Pnictides and Chalcogenides *Eur. Phys. J. B* **2014**, *87*,42.

3 Powell, A. V.; Vaqueiro, P. Chalcogenide thermoelectric materials, *RSC Energy Environ. Ser.*, **2017**, *17*, 27-59.

4 Chetty, R. ; Bali, A.; Mallik, R. C. Tetrahedrites as Thermoelectric Materials: an Overview *J. Mater. Chem. C* **2015**, *3*, 12364-12378.

5 Makovicky, E. Crystal Structures of Sulfides and other Chalcogenides *Rev. Mineral. Geochem*. **2006**, *61*, 7-125.

6 Johnson, N.E.; Craig, J. R.; Rimstidt, J. D. Crystal Chemistry of Tetrahedrite *Am. Mineral.* **1988**, *73*, 389-397.

7 Lu, X.; Morelli, D. T., Natural Mineral Tetrahedrite as a Direct Source of Thermoelectric Materials *Phys. Chem. Chem. Phys.* **2013**, *15*, 5762-5766.

8 Lu, X.; Morelli, D. T.; Xia, Y; Zhou, F.; Ozolins, V.; Chi, H.; Zhou, X. Y.; Uher, C. High Performance Thermoelectricity in Earth-Abundant Compounds Based on Natural Mineral Tetrahedrites *Adv. Energy Mater.* **2013**, *3*, 342–348.

9 Suekuni, K.; Tsuruta, K.; Kunii, M.; Nishiate, H.; Nishibori, E.; Maki, S.; Ohta, M.; Yamamoto, A.; Koyano, M. High-Performance Thermoelectric Mineral $Cu_{12-x}Ni_xSb_4S_{13}$ Tetrahedrite *J. Appl. Phys*. **2013**, *113*, 043712.

10 Suekuni, K.; Tomizawa, Y.; Ozaki, T.; Koyano, M. Systematic Study of Electronic and Magnetic Properties for $Cu_{12-x}TM_xSb_4S_{13}$ (TM=Mn, Fe, Co, Ni, and Zn) Tetrahedrite *J. Appl. Phys*. **2014**, *115*, 143702.

11 Heo, J.; Laurita, G.; Muir, S.; Subramanian, M. A.; Kesler, D. A. Enhanced Thermoelectric Performance of Synthetic Tetrahedrites *Chem. Mater.* **2014**, *26*, 2047-2051

12 Suekuni, K.; Tsuruta, K.; Ariga, T.; Koyano, M. Thermoelectric Properties of Mineral Tetrahedrites $Cu_{10}Tr_2Sb_4S_{13}$ with Low Thermal Conductivity *Appl. Phys. Express* **2012**, *5*, 051201.

13 Barbier, T.; Lemoine, P.; Gascoin, S.; Lebedev, O. I.; Kaltzoglou, A.; Vaqueiro, P.; Powell, A. V.; Smith, R. I.; Guilmeau, E. Structural Stability of the Synthetic Thermoelectric Ternary and Nickel-Substituted Tetrahedrite Phases *J. Alloys Comp*. **2015**, *634*, 253–262.

14 Lu, X.; Morelli, D. T. The Effect of Te Substitution for Sb on Thermoelectric Properties of Tetrahedrite *J. Elect. Mater.* **2014**, *43*, 1983-1987.

15 Lu, X.; Morelli, D. T.; Wang, Y.; Lai, W.; Xia, Y.; Ozolins, V. Phase Stability, Crystal Structure, and Thermoelectric Properties of $Cu_{12}Sb_4S_{13-x}Se_x$ Solid Solutions *Chem. Mater.* **2016**, *28*, 1781-1786.

16 May, A. F.; Delaire, O.; Niedziela, J. L.; Lara-Curzio, E.; Susner, M. A.; Abernathy, D. L.; Kirkham, M.; McGuire, M. A. Structural Phase Transition and Phonon Instability in $Cu_{12}Sb_4S_{13}$ *Phys. Rev. B* **2016**, *93*, 064104.

17 Tanaka, H. I.; Suekuni, K.; Umeo, K.; Nagasaki, T.; Sato, H.; Kutluk, G.; Nishibori, E.; Kasai, H.; Takabatake, T. Metal-Semiconductor Transition Concomitant with a Structural Trans-

formation in Tetrahedrite $Cu_{12}Sb_4S_{13}$ *J. Phys. Soc. Jpn.* **2016**, *85*, 014703.

18 Tatsuka, K.; Morimoto, N. Tetrahedrite Stability Relations in Cu-Sb-S System *Econ. Geol.* **1977**, *72*, 258-270.

19 Johnson, M. L.; Jeanloz, R. A. Brillouin-zone model for compositional variation in tetrahedrite *Am. Mineral.* **1983**, *68*, 220-226.

20 Bullett, D. W.; Dawson, W. G. Bonding Relationships in some Ternary and Quaternary Phosphide and tetrahedrite structures- $[Ag_6M_4P_{12}]M_6'$, $Cu_{12+x}Sb_4S_{13}$ and Cu_{14-x} Sb_4S_{13}, $Ln_6Ni_6P_{17}$ *J. Phys. C: Solid State Phys.* **1986**, *19*, 5837-5847.

21 Details of the Mantid High-Performance Computing Project may be found at http://www.mantidproject.org

22 Larson, A.C.; von Dreele, R. B. General Structure Analysis System, Los Alamos Laboratory, [Report LAUR 85-748] 1994.

23 Cowan, R. D. Pulse Method of Measuring Thermal Diffusivity at High Temperatures *J. Appl. Phys.* **1963**, *34*, 926-928.

24 Pfitzner, A.; Evain, M.; Petricek, V. $Cu_{12}Sb_4S_{13}$: A Temperature-Dependent Structure Investigation *Acta Cryst. B* **1997**, *53*, 337-345.

25 Makovicky, E.; Skinner, B. J. Studies of the Sulfosalts of Copper; VII. Crystal Structures of the Exsolution Products $Cu_{12.3}Sb_4$ S_{13} and $Cu_{13.8}Sb_4S_{13}$ of Unsubstituted Synthetic Tetrahedrite *Can. Mineral.* **1979**, *17*, 619-634.

26 Andreasen, J. W.; Makovicky, E.; Lebech, B.; Moller, S. K. The Role of Iron in Tetrahedrite and Tennantite Determined by Rietveld Refinement of Neutron Powder Diffraction Data *Phys. Chem. Minerals* **2008**, *35*, 447-454.

27 Evans, H. T.; Konnert, J. A. Crystal Structure Refinement of Covellite *Am. Mineral.* **1976**, *61*, 996-1000.

28 Garin, J.; Parthé, E. The Crystal Structure of Cu_3PSe_4 and other Ternary Normal Tetrahedral Structure Compounds with Composition $_{1}56_4$ *Acta Cryst. B* **1972**, *28*, 3672-3674.

29 Pfitzner, A. $Cu3SbS_3$ Crystal Structure and Polymorphism *Z Anorg. Allg Chem.* **1994**, *620*, 1992-1997.

30 Janosi, A. La Structure du Sulfure Cuivreux Quadratique *Acta Cryst.* **1964**, *17*, 311-312.

31 Yamamoto, K.; Kashida, S. X-ray Study of the Average Structures of Cu_2Se and $Cu_{1.8}S$ in the Room Temperature and the High Temperature Phases *J. Solid State Chem.* **1991**, *93*, 202-211.

32 Makovicky, E.; Skinner, B. J. Studies of the Sulfosalts of Copper; VI. Low-Temperature Exsolution in Synthetic Tetrahedrite Solid Solution, $Cu_{12+x}Sb_{4+y}S_{13}$ *Can. Mineral.* **1978**, *16*, 611-623.

33 Bouyrie, Y.; Candolfi, C.; Dauscher, A.; Malaman, B.; Lenoir, B. Exsolution Process as a Route toward Extremely Low Thermal Conductivity in $Cu_{12}Sb_{4-x}Te_xS_{13}$ Tetrahedrites *Chem. Mater.* **2015**, *27*, 8354-8361.

34 Pfitzner, A. Disorder of Cu^+ in Cu_3SbS_3: Structural Investigations of the High- and Low-Temperature Modification *Z. Kristallogr.* 1998, **213**, 228-236.

35 Makovicky, E. The Phase Transformations and Thermal Expansion of the Solid Electrolyte Cu_3BiS_3 between 25 and 300°C *J. Solid State Chem.*, 1983, **49**, 85-92.

36 Kirkham, M.; Majsztrik, P.; Skoug, E.; Morelli, D.; Wang, H.; Porter, W. D.; Payzant, E. A.; Lara-Curzio, E. High-Temperature Order/Disorder Transition in the Thermoelectric Cu_3SbSe_3 *J. Mater. Res.* **2011**, *26*, 2001-2005.

37 Sales, B. C.; Mandrus, D. G.; Chakoumakos, B. C. Use of atomic displacement parameters in thermoelectric materials research *Semiconduct. Semimet.* **2001**, *70*, 1-36.

38 Lara-Curzio, E.; May, A. F.; Delaire, O.; McGuire, M. A.; Lu, X.; Liu, C.-Y.; Case, E. D.; Morelli, D. T. Low-Temperature Heat Capacity and Localized Vibrational Modes in Natural and Synthetic Tetrahedrites *J. Appl. Phys.* **2014**, *115*, 193515.

39 Lai, W.; Wang, Y.; Morelli, D. T.; Lu, X. From Bonding Asymmetry to Anharmonic Rattling in $Cu_{12}Sb_4S_{13}$ Tetrahedrites: When Lone-Pair Electrons Are Not So Lonely *Adv. Funct. Mater.* **2015**, *25*, 3648-3657.

40 Qiu, W.; Xi, L.; Wei, P.; Ke, X.; Yang, J.; Zhang, W. Part-Crystalline Part-Liquid State and Rattling-Like Thermal Damping in Materials with Chemical-Bond Hierarchy *PNAS* **2014**, *111*, 15031.

41 G. Guélou, PhD thesis, University of Reading, 2016.

42 Lemoine, P.; Bourgès, C.; Barbier, T.; Nassif, V.; Cordier, S.; Guilmeau, E. High temperature neutron powder diffraction study of the $Cu_{12}Sb_4S_{13}$ and $Cu_4Sn_7S_{16}$ phases, *J. Solid State Chem.* **2017**, *247*, 83-89.

43 Bhattacharya, S.; Basu, R.; Bhatt, R.; Pitale, S.; Singh, A.; Aswal, D. K.; Gupta, S. K.; Navaneethan, M.; Hayakawa, Y. Cu-$CrSe_2$: a High Performance Phonon Glass and Electron Crystal Thermoelectric Material *J. Mater. Chem. A* **2013**, *1*, 11289-11294.

44 Weldert, K. S.; Zeier, W. G.; Day, T. W.; Panthöfer, M.; Snyder, G. J.; Tremel, W. Thermoelectric Transport in Cu_7PSe_6 with High Copper Ionic Mobility *J. Am. Chem. Soc.* **2014**, *136*, 12035-12040.

45 Li, L.; Liu, Y.; Dai, J.; Hong, A.; Zeng, M.; Yan, Z.; Xu, J.; Zhang, D.; Shan, D.; Liu, S.; Ren, Z.; Liu, J.-M. High Thermoelectric Performance of Superionic Argyrodite Compound Ag_8SnSe_6 *J. Mater. Chem. C* **2016**, *4*, 5806-5813.

46 Bouyrie, Y.; Candolfi, C.; Ohorodniichuk, V.; Malaman, B.; Dauscher, A.; Tobola, J.; Lenoir, B. Crystal Structure, Electronic Band Structure and High-Temperature Thermoelectric Properties of Te-Substituted Tetrahedrites $Cu_{12}Sb_{4-x}Te_xS_{13}$ ($0.5 \leq x \leq 2.0$) *J. Mater. Chem. C* **2015**, *3*, 10476-10487.

47 Cahill, D. G.; Watson, S. K.; Pohl, R. O. Lower Limit to the Thermal Conductivity of Disordered Crystals *Phys. Rev. B* **1992**, *46*, 6131-6140.

48 Murashov, V.; White, M. A. in *Thermal Conductivity: Theory, Properties and Applications*, Chapter 3, Ed. T. M. Tritt, Springer 2004.

49 Suekuni, K.; Tanaka, H. I.; Kim, F. S.; Umeo, K.; Takabatake, T. Glasslike versus Crystalline Thermophysical Properties of the Cu-S based Minerals: Tetrahedrite and Colusite *J. Phys. Soc. Jpn.* **2015**, *84*, 103601.

50 Sales, B. C.; Mandrus, D.; Williams, R. K. Filled Skutterudite Antimonides: A New Class of Thermoelectric Materials *Science* **1996**, *272*, 1325-1328.